

2-7-2024

Meso-fracture evolution characteristics of freeze-thawed sandstone based on discrete element method simulation

Yong-jun SONG

College of Architecture and Civil Engineering, Xi'an University of Science and Technology, Xi'an, Shaanxi 710054, China, songyj79@xust.edu.cn

Yin-wei SUN

College of Architecture and Civil Engineering, Xi'an University of Science and Technology, Xi'an, Shaanxi 710054, China, sunyinwei2021@163.com

Chen-jing LI

College of Architecture and Civil Engineering, Xi'an University of Science and Technology, Xi'an, Shaanxi 710054, China

Hui-min YANG

College of Architecture and Civil Engineering, Xi'an University of Science and Technology, Xi'an, Shaanxi 710054, China

See next page for additional authors

Follow this and additional works at: <https://rocksoilmech.researchcommons.org/journal>



Part of the [Geotechnical Engineering Commons](https://rocksoilmech.researchcommons.org/journal)

Recommended Citation

SONG, Yong-jun; SUN, Yin-wei; LI, Chen-jing; YANG, Hui-min; ZHANG, Lei-tao; and XIE, Li-jun (2024) "Meso-fracture evolution characteristics of freeze-thawed sandstone based on discrete element method simulation," *Rock and Soil Mechanics*: Vol. 44: Iss. 12, Article 7.

DOI: 10.16285/j.rsm.2023.5448

Available at: <https://rocksoilmech.researchcommons.org/journal/vol44/iss12/7>

This Article is brought to you for free and open access by Rock and Soil Mechanics. It has been accepted for inclusion in Rock and Soil Mechanics by an authorized editor of Rock and Soil Mechanics.

Meso-fracture evolution characteristics of freeze-thawed sandstone based on discrete element method simulation

Abstract

To investigate the mesoscopic damage accumulation and the loading-induced fracture process in freeze-thawed rocks, a method coupling water-ice particle phase transition and expansion based on the discrete element method is proposed. The rock freeze-thaw process is simulated using a particle flow program, and the reliability of the simulation results is verified through laboratory experiments. The frost heave evaluation index of pore water particles is quantitatively characterized, and a functional relationship between and the number of freeze-thaw cycles N is established. Furthermore, the fracture characteristics and the evolution of microcrack, displacement field and force chain field in freeze-thawed rocks during the loading process are evaluated. The results show that: (1) The volumetric expansion of pore water in the rock and continuous water replenishment are the essential causes of rock damage under freeze-thaw treatments. Microcracks in the samples are dominated by tensile cracks during the freeze-thaw process, exhibiting an “initially slow, then fast” evolutionary trend, with more significant displacement of rock particles on the periphery than those in the interior. (2) The number of microcracks in the samples under loading exhibits a “slow→gradual→rapid” growth trend. The numbers of freeze-thaw cycles positively correlated with the number of microcracks but negatively correlated with the microcrack initiation stress. (3) The fracture process and morphology of the samples differ significantly before and after freeze-thaw treatment. When the load approaches the peak stress, there are “abnormal signals” in the microcrack distribution, displacement field and force chain field, which can serve as a precursor to failure identification. Under the influence of freeze-thaw cycles, the spatial arrangement of microcracks inside the samples becomes more complex, and the fracture mode transitions from dominance by tensile microcracks to dominance by mixed tensile-shear microcracks. This study provides a new idea and method for exploring the failure behavior of freeze-thawed rocks.

Keywords

discrete element method, freeze-thaw cycles, particle flow, mesoscopic damage, uniaxial compression, fracture evolution

Authors

Yong-jun SONG, Yin-wei SUN, Chen-jing LI, Hui-min YANG, Lei-tao ZHANG, and Li-jun XIE

Meso-fracture evolution characteristics of freeze-thawed sandstone based on discrete element method simulation

SONG Yong-jun¹, SUN Yin-wei¹, LI Chen-jing¹, YANG Hui-min¹, ZHANG Lei-tao², XIE Li-jun³

1. College of Architecture and Civil Engineering, Xi'an University of Science and Technology, Xi'an, Shaanxi 710054, China

2. School of Civil Engineering, Dalian University of Technology, Dalian, Liaoning 116024, China

3. China Metallurgical Group Northwest Geotechnical Engineering Co., Ltd., Xi'an, Shaanxi 710061, China

Abstract: To investigate the mesoscopic damage accumulation and the loading-induced fracture process in freeze-thawed rocks, a method coupling water-ice particle phase transition and expansion based on the discrete element method is proposed. The rock freeze-thaw process is simulated using a particle flow program, and the reliability of the simulation results is verified through laboratory experiments. The frost heave evaluation index λ_v of pore water particles is quantitatively characterized, and a functional relationship between λ_v and the number of freeze-thaw cycles N is established. Furthermore, the fracture characteristics and the evolution of microcrack, displacement field and force chain field in freeze-thawed rocks during the loading process are evaluated. The results show that: (1) The volumetric expansion of pore water in the rock and continuous water replenishment are the essential causes of rock damage under freeze-thaw treatments. Microcracks in the samples are dominated by tensile cracks during the freeze-thaw process, exhibiting an “initially slow, then fast” evolutionary trend, with more significant displacement of rock particles on the periphery than those in the interior. (2) The number of microcracks in the samples under loading exhibits a “slow→gradual→rapid” growth trend. The numbers of freeze-thaw cycles positively correlated with the number of microcracks but negatively correlated with the microcrack initiation stress σ_i . (3) The fracture process and morphology of the samples differ significantly before and after freeze-thaw treatment. When the load approaches the peak stress σ_r , there are “abnormal signals” in the microcrack distribution, displacement field and force chain field, which can serve as a precursor to failure identification. Under the influence of freeze-thaw cycles, the spatial arrangement of microcracks inside the samples becomes more complex, and the fracture mode transitions from dominance by tensile microcracks to dominance by mixed tensile-shear microcracks. This study provides a new idea and method for exploring the failure behavior of freeze-thawed rocks.

Keywords: discrete element method; freeze-thaw cycles; particle flow; mesoscopic damage; uniaxial compression; fracture evolution

1 Introduction

Rock is a typical heterogeneous geological material composed of cemented mineral particles and various types of micro-defects, such as micropores and microcracks. These defects serve as channels for water to enter the interior of rock^[1–2]. In cold regions, significant temperature variations due to seasonal changes and diurnal cycles result in long-term freeze-thaw weathering of near-surface rocks^[3], causing a rapid deterioration in their physico-mechanical properties^[4]. In fact, the freeze-thaw weathering failure of rocks is mainly caused by the frost heave pressure generated by the frequent freezing/thawing process of internal pore water^[5]. When the frost heave pressure exceeds the tensile strength of the rock, new microcracks develop, gradually reducing the strength of the rock, thereby posing a significant threat to the stability of rock engineering in cold regions^[6–8]. Therefore, conducting research on the mesoscopic damage evolution and failure behavior of rocks under cyclic freeze-thaw conditions

is of significant practical guidance.

The mechanical properties of rocks in cold regions under freeze-thaw environments have attracted considerable attention for a long time. Previous studies have indicated a significant impact of freeze-thaw action on the physico-mechanical properties of rocks^[9–11]. However, considering that the damage caused by freeze-thaw weathering mainly manifests as the initiation, propagation, and connection of internal microcracks^[12], these internal evolutionary behaviors are a challenging to reveal from a macroscopic perspective. Therefore, numerous scholars have conducted extensive research at the mesoscopic level. Martínez-Martínez et al.^[13] conducted freeze-thaw experiments on carbonate rocks, and they used scanning electron microscopy to examine the evolution of the microscopic structure of rocks after freeze-thaw treatment. Song et al.^[14] conducted freeze-thaw tests on fractured sandstone in both saturated water and saturated ice conditions and analyzed the characteristics of secondary fracture evolution under freeze-thaw condition using CT scanning. Jiang et al.^[15]

Received: 11 April 2023

Accepted: 23 May 2023

This work was supported by the National Natural Science Foundation of China (42277182, 11972283).

First author: SONG Yong-jun, male, born in 1979, PhD, Professor, PhD supervisor, mainly engaged in the research and teaching works on rock mechanics and underground engineering. E-mail: songyj79@xust.edu.cn

Corresponding author: SUN Yin-wei, male, born in 1999, Master's student, focusing on rock mechanics. E-mail: sunyinwei2021@163.com

investigated the damage of sandstone during the freeze-thaw process under different hydration environments using nuclear magnetic resonance and acoustic emission techniques. Chen et al.^[16] analyzed the formation of cracks in freeze-thawed rocks using laser scanning microscopy and found that the depth, width, and surface area ratio of cracks all increase with the number of freeze-thaw cycles. The above studies have made gratifying progress, but there are still challenges in accurately observing and characterizing the generation and local evolution of internal microcracks during cyclic freeze-thaw conditions. However, with the development of advanced numerical techniques, new solutions have been found in addressing this issue.

Numerical technology is a crucial means for studying the complex mechanical behaviors of rocks and provides an effective approach to addressing issues such as rock fracturing^[17–18]. Existing numerical methods mainly focus on finite element methods and discrete element methods. Due to the limitation of continuity assumption, finite element methods usually cannot directly capture the process of crack initiation and propagation inside rocks^[19]. In contrast, discrete element methods can reproduce the entire process of microcrack development inside rocks from a mesoscopic perspective, presenting certain advantages relative to finite element methods^[20–21]. Based on the discrete element method, the particle flow method has been widely applied in the study of rock mechanics problems. Zhou et al.^[22] analyzed the internal strain evolution and crack propagation mechanism of granite under ultrahigh-frequency fatigue loads through laboratory experiments and PFC^{2D} numerical simulations. Xiong et al.^[23] used a particle flow program to simulate sandstone with intersecting cracks and investigated the fracture characteristics of samples under the influence of intersecting cracks. Bian et al.^[24], based on PFC^{2D}, simulated the unloading process of shale samples under different water absorption times, revealing the evolution of internal cracks at different unloading stages. Wu et al.^[25] conducted numerical tests on anchored fractured rock samples and studied the impact of different anchoring angles on crack propagation in the sample. Although the application of numerical methods to the study of freeze-thawed rocks has been proposed previously^[26], unfortunately, there is currently a lack of attention to the mesoscopic damage evolution during the freeze-thaw process. Additionally, it remains unclear how the internal microcracks, displacement field, and force chain field evolve and result in macroscopic fracture characteristics in freeze-thawed rocks under loading conditions.

Based on the above considerations, a method coupling water-ice particle phase transition and expansion is proposed in this paper. The numerical model of freeze-thawed

sandstone is established using the particle flow program, and the mesoscopic parameters of the model are calibrated based on indoor tests. The Fish code is employed to simulate the freeze-thaw process. The simulation results are validated through indoor experiments. The frost heave evaluation index of pore water particles is quantitatively characterized, and the evolution of internal microcracks and the fracture evolution law of freeze-thawed rocks under loading conditions are investigated.

2 Indoor test

To provide a basis for the calibration of mesoscopic parameters in the numerical model and to assess the reliability of simulation results, indoor tests were initially conducted. The white sandstone used in this study was sampled from a site in western China and processed into standard samples with dimensions of 50 mm×100 mm (diameter×height). Based on the measured longitudinal wave velocity and natural density, the samples with significant differences were excluded. After drying and saturating the selected samples, the following mean physical parameters were obtained as follows: the dry density is 2.294 g/cm³, the saturated density is 2.413 g/cm³, and the saturation moisture content is 5.19%. The following experiments were carried out:

(1) Cyclic freeze-thaw test. According to *Standard for test methods of engineering rockmass* (GB/T50266—2013)^[27], initially, the saturated samples were sealed with a thin film to ensure moisture retention during the freezing process. They were then placed in a low-temperature device for freezing and subsequently thawed by placing them in a water-containing container. According to the temperature variations in cold regions^[28], the temperature range for the freeze-thaw treatment was set between –20 °C and +20 °C, with each cycle lasting 24 hours (see Fig. 1(b)). 0, 10, 20, and 30 freeze-thaw cycles were considered. After reaching the specified number of freeze-thaw cycles (10, 20, 30), the moisture content of the samples was measured and the average values were 5.32%, 5.76%, and 6.30%, respectively.

(2) Uniaxial compression test. The loading equipment is the TAW-1000 computer-controlled rock mechanics servo testing machine, as shown in Fig. 1(c). Mechanical tests were conducted on the rock samples subjected to different numbers of freeze-thaw cycles.

Figure 2 presents the uniaxial compressive stress–strain curves of sandstone corresponding to different numbers of freeze-thaw cycles. It can be observed that the deformation and failure of the samples roughly go through four stages, namely compaction stage, elastic stage, plastic stage, and

post-peak stage. Additionally, it is evident that as the number of freeze-thaw cycles increases, the stress–strain curve shows three significant changes. (i) The compaction stage of the stress–strain curve becomes longer, and the nonlinear compaction characteristics become more pronounced. (ii) The slope of the stress–strain curve in the linear elastic

stage decreases, and the peak stress decreases. (iii) The decrease in post-peak stress gradually slows down, and the ductility increases. These features indicate that the freeze-thaw process leads to an increase in micropores and microcracks inside the rock samples, and the internal damage gradually accumulates.

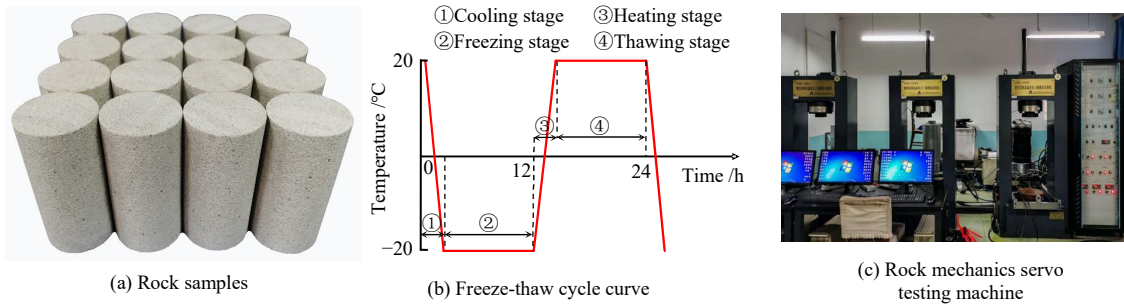


Fig. 1 Indoor test

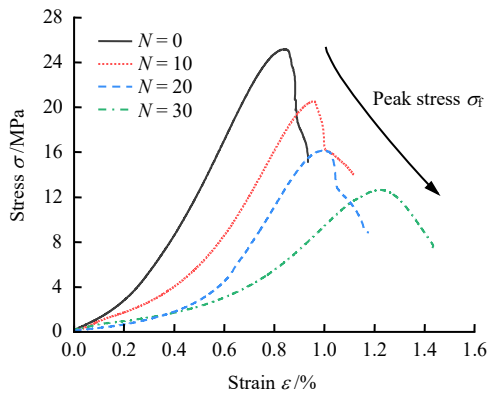


Fig. 2 Stress–strain curves of sandstone corresponding to different numbers of freeze-thaw cycles

According to the suggested method of ISRM^[29], the approximately linear portion of the stress–strain curve before the peak in Fig. 2 is selected to calculate the elastic modulus E , and both the peak strength and E are plotted in Fig. 3. As shown in the figure, it is evident that the peak strength σ_f and E both show a decreasing trend with an increasing number of freeze-thaw cycles (N). However, the difference lies in the fact that σ_f decreases linearly, while E exhibits an upward convex exponential decay. Specifically, for the sample without freeze-thaw treatment, σ_f is 25.16 MPa. After 10, 20, and 30 freeze-thaw treatments, σ_f decreases by 4.64, 9.0, and 12.51 MPa, respectively, with strength loss rates of 18.44%, 35.77%, and 49.72%. As N increases from 0 to 30, E decreases from 4.35 GPa to 1.89 GPa, with a reduction of 57%, indicating that the freeze-thaw action significantly weakens the deformation resistance of rocks. The continuous decrease in σ_f and E reflects that the deterioration inside rocks caused by the freeze-thaw action is gradually accumulated, and it is difficult to evaluate the mesoscopic damage caused

by freeze-thaw weathering solely from physical experiments. Therefore, numerical tools are necessary to assist in indoor experimental analysis and research.

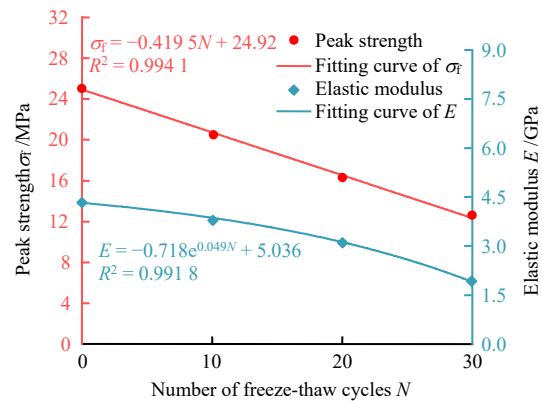


Fig. 3 Relationship between peak strength, elastic modulus and number of freeze-thaw cycles

3 Numerical realization of freeze-thaw process

3.1 Particle flow method (PFC^{3D})

The bonded particle model (BPM), initially proposed by Potyondy et al.^[30] based on the discrete element method (DEM), can be implemented in Particle Flow Code (PFC). Specifically, the parallel bond model (PBM) is a type of BPM, which has been proven to be more suitable for reflecting the mechanical behavior of rock materials^[31].

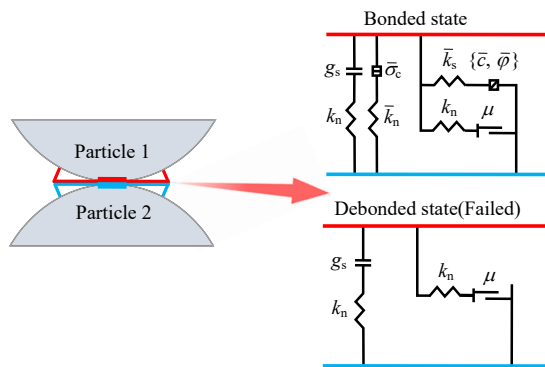
Figure 4(a) depicts the schematic diagram of PBM. When particles are in a bonded state, both linear and parallel bond elements work together to resist force and moment. When bond failure occurs and the system transitions to a debonded (failed) state, only the linear elements remain active, leading the PBM to degenerate into a linear model.

The PBM strength envelope is illustrated in Fig. 4(b), with the stress expressions given by:

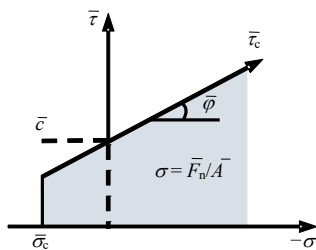
$$\bar{\sigma} = \frac{\bar{F}_n}{\bar{A}} + \beta \frac{\|\bar{M}_b\| \bar{R}}{\bar{I}} \quad (1)$$

$$\bar{\tau} = \frac{\|\bar{F}_s\|}{\bar{A}} + \beta \frac{\|\bar{M}_t\| \bar{R}}{\bar{J}} \quad (2)$$

where \bar{F}_n is the normal parallel bond force, \bar{F}_s is the tangential parallel bond force, \bar{M}_t and \bar{M}_b are the rotational torque and bending moment on the contact plane, \bar{R} is the particle radius, \bar{A} is the cross-sectional area, β is the moment contribution coefficient, and \bar{I} and \bar{J} are the moment of inertia and polar moment of inertia. When $\bar{\sigma} \geq \bar{\sigma}_c$, tensile failure occurs, leading to tensile cracks. When $\bar{\tau} \geq \bar{\tau}_c$, shear failure occurs, resulting in shear cracks.



(a) Schematic diagram



(b) Strength envelope

Fig. 4 Parallel bond model (modified from PFC manual^[32])

3.2 Freeze-thaw simulation

The freeze-thaw failure of rock is usually caused by the volume changes resulting from the repeated liquid-ice phase transitions of pore water^[33]. As shown in Fig. 5, during the freezing state, water turns into ice, leading to volume expansion and generating frost heave pressure. The mineral particles around the pores in the rock are compressed by the pressure, causing interparticle debonding and fracturing. In the subsequent thawing state, the ice turns back into water, which is reabsorbed into the pores, preparing for the next freezing stage. After repeated freeze-thaw cycles, irreversible freeze-thaw damage occurs inside the rock, resulting in a deterioration in its mechanical properties.

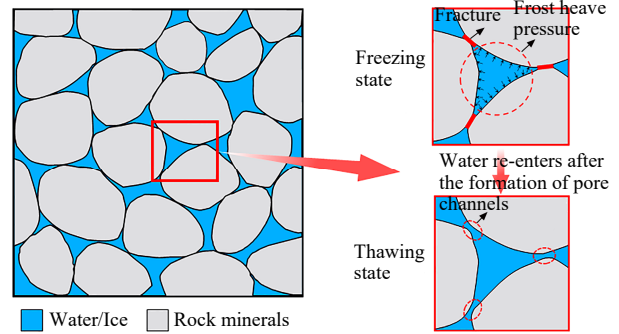


Fig. 5 Meso-damage diagram of freeze-thawed rock

Through the aforementioned analysis of the mesoscopic damage of rock caused by freeze-thaw, a method coupling water-ice particle phase transition and expansion is proposed based on the discrete element method. Utilizing the particle flow code, the cyclic freezing and thawing process of rock is simulated under the following assumptions:

(1) The model of saturated sandstone sample is simplified to be composed of rock mineral particles and pore water particles.

(2) The seepage of pore water inside the rock during the freeze-thaw process is disregarded.

(3) The temperature of pore water particles vary synchronously with the ambient temperature during heating or cooling.

In a single freeze-thaw cycle, the initial volume of an individual pore water particle can be represented by the following equation:

$$V_0 = \frac{4}{3} \pi r_0^3 \quad (3)$$

where r_0 is the initial radius of the pore water particle, and the volume of a single pore water particle after freezing can be expressed by the following equation:

$$V_F = \frac{4}{3} \pi (r_0 + u_v)^3 = V_0 + \Delta V_w \quad (4)$$

where $\Delta V_w = 4\pi(r_0^2 u_v + r_0 u_v^2 + 1/3 u_v^3)$ is the volume increment of pore water particles after freezing, u_v is the expansion of pore water particle radius. According to the research by Liu et al.^[34] on the frost heave model of rock pores at low temperatures, u_v is calculated using the following equation:

$$u_v = r_0 \frac{p_i}{E_m} \frac{[1 + v_m + 2(1 - 2v_m)n]}{2(1 - n)} \quad (5)$$

$$p_i = \frac{0.029}{\frac{1}{E_m} \frac{1 + 2n + (1 - 4n)v_m}{2(1 - n)} + 1.029 \frac{1 - 2v_i}{E_i}} \quad (6)$$

where E_m and v_m are the elastic modulus and Poisson's ratio of the rock matrix; E_i and v_i are the elastic modulus

and Poisson’s ratio of the pore ice, with values of 9 GPa and 0.35, respectively; n is the porosity of the rock; and p_i is the pore ice pressure in the rock.

The relationship between particle volume and unfrozen water content during the freeze-thaw process of a single pore water particle can be expressed by the following equation:

$$V = \begin{cases} V_0 + \Delta V_w(1 - w_u) & T \leq 0^\circ\text{C} \\ V_0 & T > 0^\circ\text{C} \end{cases} \quad (7)$$

where V is the volume of the pore water particle at arbitrary temperature; and w_u is the unfrozen water content, which can be calculated by the following equation^[34]:

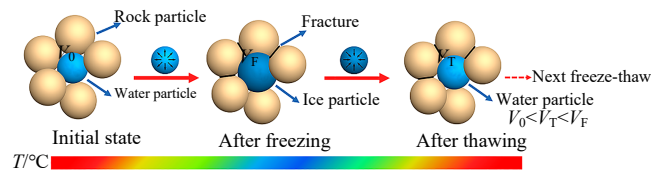
$$w_u = \begin{cases} 1 - \left[1 + 0.139 \left(\frac{1}{\Delta T} \right)^{1/3} \ln \left(\frac{1 + e^{-0.268\Delta T}}{2} \right) \right] (1 - e^{-0.268\Delta T}) & (\Delta T > 0) \\ 1 & (\Delta T \leq 0) \end{cases} \quad (8)$$

where $\Delta T = T_m - T$, T_m is the freezing point of free water at atmospheric pressure, with a standard value of 273.15 K, and T is the temperature obtained currently.

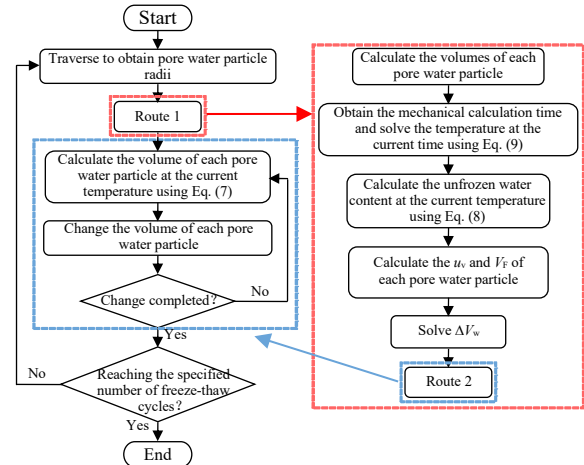
According to the assumptions for the numerical simulation, when the ambient temperature is cooled or heated to the specified temperature, all pore water particles in the sample reach the target temperature synchronously. Therefore, the ambient temperature is no longer kept constant after reaching the target temperature during the freeze-thaw cycle. Combining with the natural variation law of temperature over time in the environment^[35], the relationship between temperature and time is expressed using a cosine function:

$$T = 20 \cos\left(\frac{\pi t}{30}\right) \quad (9)$$

The above formulas describe the phase transition process of a single pore water particle during freezing and thawing, and the variation of pore water particle state is illustrated in Fig. 6(a). The entire freeze-thaw cycle of the sample is realized by Fish code, which controls the water-ice particle phase transition and expansion of pore water particles with temperature changes, and the calculation flow is shown in Fig. 6(b). Additionally, the volume of pore water particles at the start of each freeze-thaw cycle is set to be greater than the volume at the end of the previous freeze-thaw cycle to simulate the water supply during the experimental freeze-thaw process.



(a) Variation of pore water particle state



(b) Flowchart of Fish code

Fig. 6 Numerical realization of freeze-thaw cycle

3.3 Model construction and parameter calibration

The numerical sample of saturated sandstone is depicted in Fig. 7, consisting of two mediums: rock particles and pore water particles. The dimensions of the numerical sample match those of the laboratory sandstone sample. To achieve an optimized model closer to reality, various attempts were made with different particle radii and volume ratios in constructing the model. The basic information of the particles in the calibrated model is shown in Table 1. It is noteworthy that, for the actual loading process in the laboratory experiment, the sample strength is provided by the sandstone skeleton. Hence, the pore water particles are removed from the numerical sample to ensure that the strength is provided by the rock particle skeleton in the numerical uniaxial compression test.

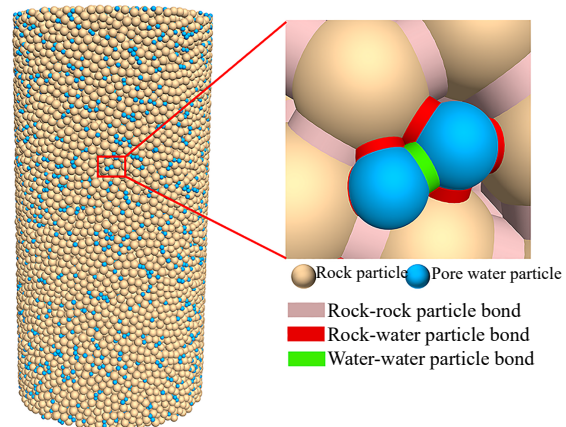


Fig. 7 Numerical sample

To simplify the parameter calibration process, it is common to keep the particle modulus (E_c) consistent with the parallel bond modulus (\bar{E}_c), and the particle stiffness ratio consistent with the parallel bond stiffness ratio^[36]. Additionally, since actual freeze-thawed damage occurs between rock skeletons, the strengths of water-water particle bonds and rock-water particle bonds should be set large enough to avoid influencing the results. Based on the laboratory test results, a trial and error method was

employed for the calibration of mesoscopic parameters, and the calibrated mesoscopic parameters are shown in Table 2.

Table 1 Meso-parameters for numerical simulation

Particle type	Particle radius /mm		Particle density /($\text{kg} \cdot \text{m}^{-3}$)
	Minimum R_{\min}	Maximum R_{\max}	
Rock particle	0.9	1.1	2.3
Pore water particle	0.5	0.6	1.0

Table 2 Meso-parameters for numerical simulation

Bond type	Contact modulus between particles E_c /GPa	Particle stiffness ratio	Frictional coefficient μ	Parallel bond modulus \bar{E}_c /GPa	Normal to tangential stiffness ratio of parallel bond \bar{k}_n / \bar{k}_s	Normal strength of parallel bond /MPa	Tangential strength of parallel bond /MPa	Friction angle of parallel bond /($^\circ$)
Rock-rock bond	2.8	3.5	0.5	2.8	3.5	6.3	10.6	30
Water-water bond	2.8	0.5	—	2.8	0.5	150.0	150.0	0
Rock-water bond	2.8	0.5	—	2.8	0.5	150.0	150.0	0

The results of the calibrated model are shown in Fig. 8. Due to the difficulty of reproducing the initial defects of natural rock samples in numerical models, there are some deviations in the simulated strain curve relative to the experimental curve. However, without considering the compaction stage^[37], the peak strength σ_f , elastic modulus E , and failure mode of the sample are in good agreement. The calibrated values are $\sigma_f = 25.18$ MPa and $E = 4.38$ GPa. In comparison, the values obtained from the laboratory test are $\sigma_f = 25.16$ MPa and $E = 4.35$ GPa, with relative errors for both parameters being less than 1%. Simultaneously, the numerical results also well reflect the post-peak stage of the curve, indicating the reasonable feasibility of the mesoscopic parameters in Table 2 for numerical tests.

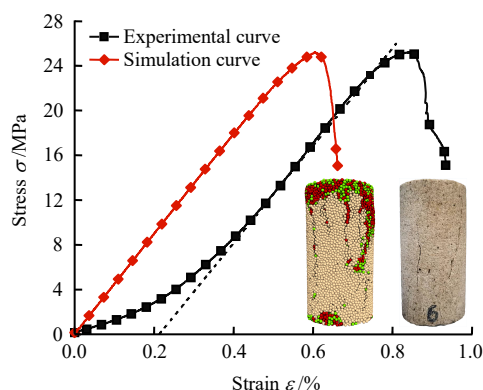


Fig. 8 Comparison of stress-strain curves and failure patterns

4 Result and analysis

4.1 Mesoscopic damage evolution analysis

Under the freeze-thaw treatment, the mesoscopic damage

evolution process of sandstone is illustrated in Fig. 9. Microcracks generated in the sample are represented in black. From the top view, it is observed that no microcracks are generated without freeze-thaw treatment. After 10 freeze-thaw cycles, a small number of microcracks first appear on the outer side of the sample. As the number of freeze-thaw cycles continues to increase, by the 20th cycle, the density of microcracks on the periphery of the sample increases, and localized crack aggregation occurs. By the 30th cycle, more microcracks appear and extend towards the inner side of the sample, intensifying the damage. These phenomena are mainly attributed to two factors:

(1) Compared to the center pore water particles, those near the periphery of the sample experience fewer constraints from the surrounding rock particles, making the surrounding rock particles easier to be fractured under the freezing-induced expansion. Hence, the density of microcracks on the periphery of the sample is higher compared to the center.

(2) As the number of freeze-thaw cycles increases, the pore water particles undergo more significant expansion. Even with more rock particles enclosing them inside the sample, it is challenging to restrain the expansion of water particles, leading to fractures in the rock particles. Therefore, the phenomenon of microcracks evolving towards the inner side is observed.

Furthermore, from the front view, it is observed that the density of surface microcracks continuously increases from 0 to 30 freeze-thaw cycles, exhibiting a local “cumulative effect”^[38]. This leads to severe deterioration of the sample, consistent with laboratory observations (see

Fig. 12). This indicates that the development of freeze-thawed damage is an accumulative process, and when the local damage accumulates to a certain extent, it can result in a significant reduction in the load-bearing capacity of the rock and even lead to failure.

In the overall perspective of the cyclic freeze-thaw process, the evolution of microcracks exhibits a “slow first and then fast” trend, indicating that the freeze-thawed damage increases sharply at the later stage. This is consistent with the CT observation reported by Tan et al.^[39]. In summary, the simulation results provide an intuitive representation of the cumulative damage process within the rock under freeze-thaw conditions.

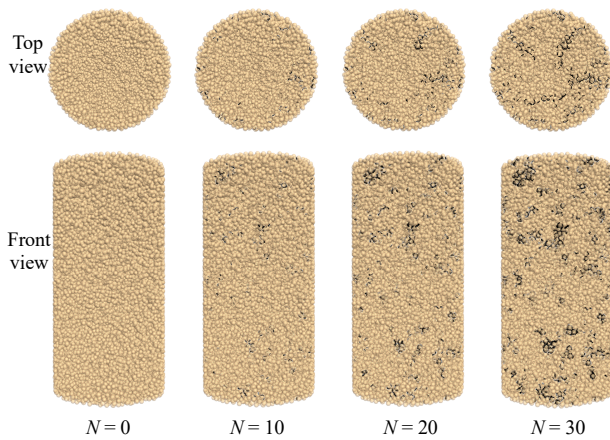


Fig. 9 Evolution of microcracks in freeze-thawed sandstone

To assess the evolution of microcracks under freeze-thaw conditions, the quantity and orientation of microcracks in the sample were statistically analyzed and depicted

in Fig. 10. In this figure, the radial axis represents the number of cracks, while the circumferential axis indicates the crack orientation.

From Fig. 10, it is evident that after 10, 20, and 30 freeze-thaw cycles, tensile microcracks are significantly more prevalent than shear microcracks. This indicates that tensile microcracks dominate the freeze-thaw cycle process, consistent with Winkler’s findings^[40] that rocks are prone to tensile failure under freeze-thaw conditions. Regarding tensile microcracks, as the cyclic freeze-thaw treatment proceeds, the quantity of microcracks gradually increases in all directions. This is mainly due to the volume expansion of pore water particles transforming into ice particles as the temperature decreases, exerting pressure on the surrounding rock particle skeleton. When the frost heave force exceeds the bonding strength between rock particles, the rock skeleton fractures, resulting in the formation of microcracks. In terms of shear microcracks, they exhibit a more disorderly pattern, with fewer in the early stages of the freeze-thaw process and a relatively faster increase in the later stages. This indicates that the damage and deterioration of the sample are more significant in the later stages of the freeze-thaw process. However, the evolution of microcracks mentioned above is not sufficient to fully reflect the impact of freeze-thaw action.

Furthermore, the displacement contours for the sample under different freeze-thaw cycles are depicted in Fig. 11. From the figure, it can be observed that in the early stages of the freeze-thaw process (see Fig. 11(a)), only partial positions in the sample experienced displacement, with

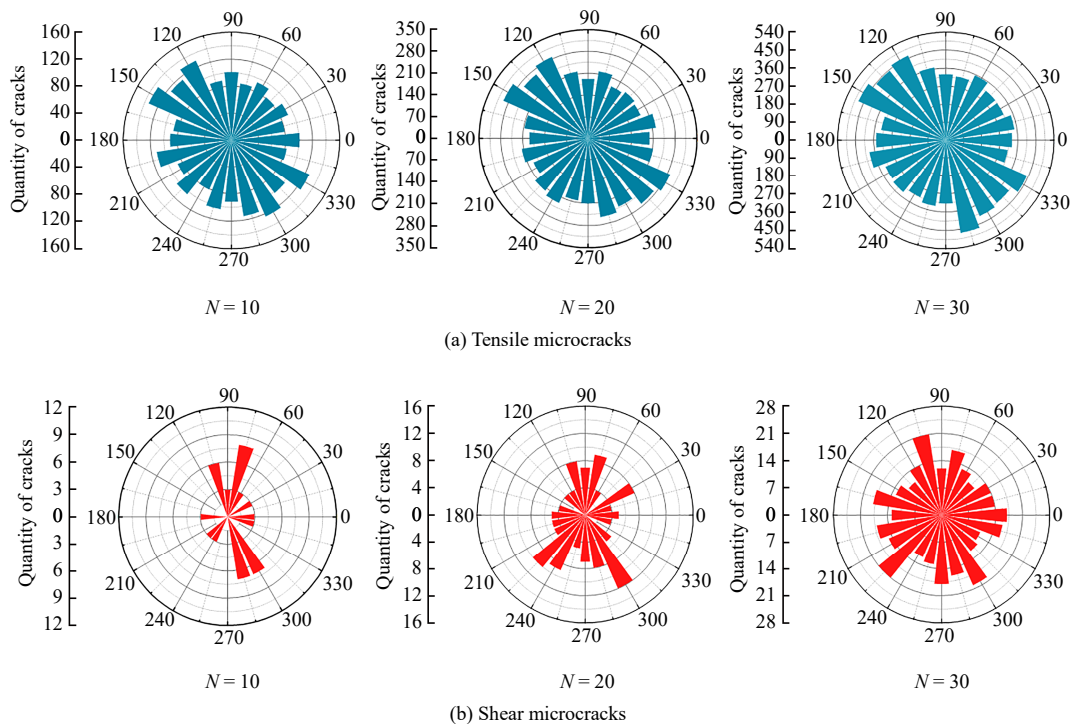


Fig. 10 Rose diagrams of sample crack under different numbers of freeze-thaw cycles

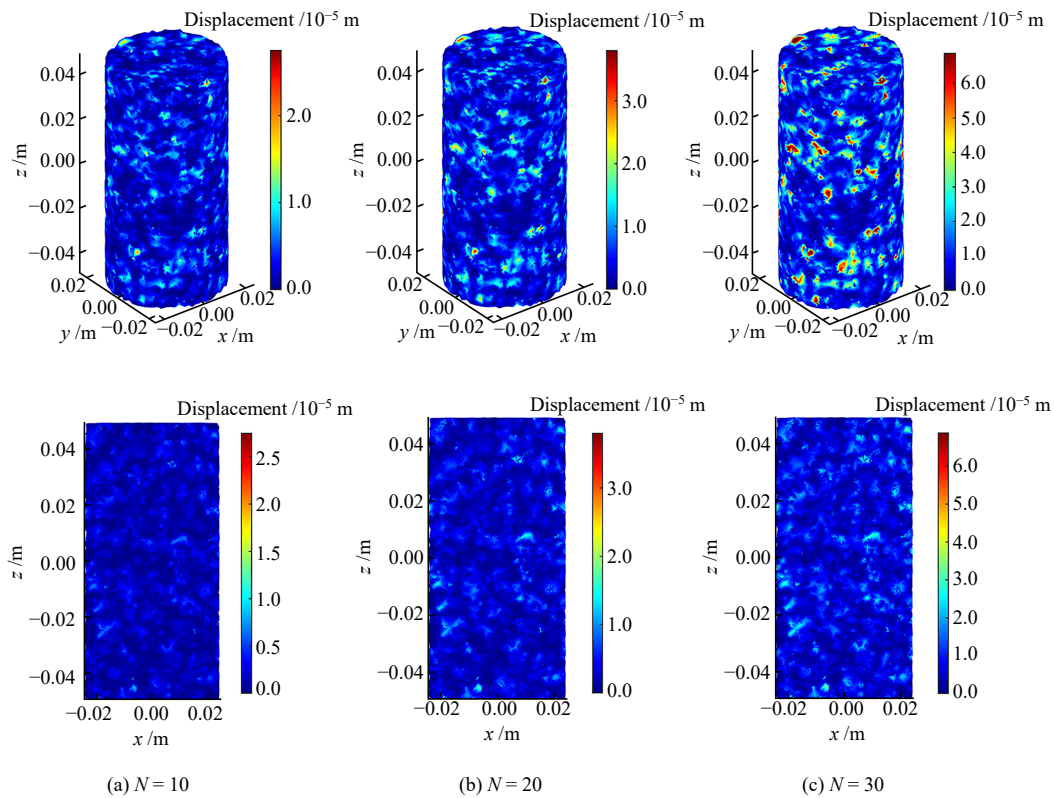


Fig. 11 Displacement contours and x - z section displacement states of samples under different numbers of freeze-thaw cycles

a maximum value of 2.89×10^{-5} m, mainly concentrated at the periphery. From the x - z cross-section view, there is almost no displacement inside the sample. As the cyclic freeze-thaw treatment proceeds, the displacement at the periphery of the sample increases further (see Fig. 11(b)), with a maximum displacement of 3.35×10^{-5} m, representing an increment of 0.46×10^{-5} m. The x - z cross-section shows that the displacement at the central region is still very small, while the particles at local areas near the periphery of the sample experience relatively large displacement. By the 30th freeze-thaw cycle (see Fig. 11(c)), the displacement at the upper and lower ends of the sample increases significantly, and surface particle displacement becomes more pronounced, with a maximum displacement of 6.88×10^{-5} m, and the displacement increment reaches up to 3.53×10^{-5} m, indicating severe rock damage.

In summary, the displacement of rock particles is more pronounced at the periphery of the sample compared to the interior, resulting in more severe deterioration at the periphery. This is consistent with the observations from laboratory experiments (see Fig. 12), where after cyclic freeze-thaw treatment, noticeable “spalling” of mineral particles on the surface of the sandstone can be observed. This is primarily attributed to the fact that rock particles near the center of the sample strongly constrained by surrounding particles, leading to relatively small displacements. In contrast, the rock particles near the sample surface are less constrained. As a result, the displacement of

peripheral particles is the largest and microcracks appear first. This is similar to the conclusion obtained by Huang et al^[41].

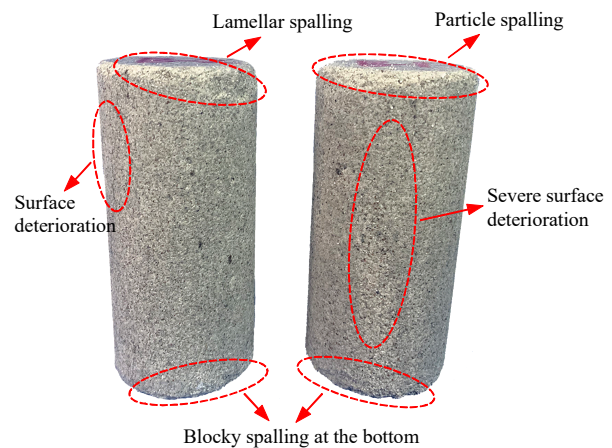


Fig. 12 Deterioration degree of sandstone after 30 freeze-thaw treatments in the laboratory

4.2 Characterization of frost heave evaluation index

To further reveal the underlying reasons for the damage and deterioration of the sample subjected to cyclic freeze-thaw treatment, Fig. 13 illustrates the volume changes of pore water particles after each freezing/thawing in the simulation.

From Fig. 13, it can be observed that in the early stage of the freeze-thaw process, the freezing-induced volume expansion of pore water particles is relatively small.

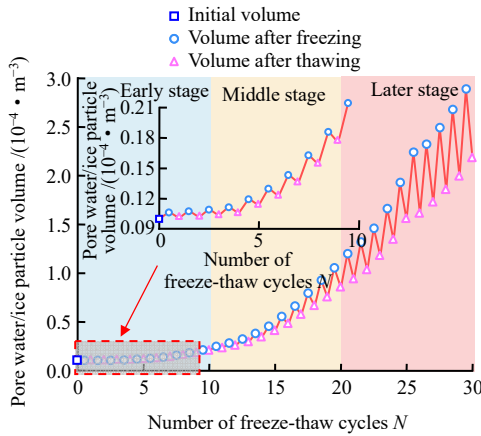


Fig. 13 Volume change of pore water/ice particles during freeze-thawing process

However, the volume expansion becomes more pronounced in the middle and later stages. This is primarily due to the fact that the internal pore water in the rock undergoes volume expansion in the frozen state, generating frost heave pressure and causing pore expansion. With an increasing number of freeze-thaw cycles, the pore volume gradually increases, allowing more water to enter. Consequently, the pore water volume expands further in the next freezing stage. It means that in the middle and later stages of the freeze-thaw process, the volume expansion of pore water particles gradually becomes more noticeable. Additionally, with each subsequent freeze-thaw cycle, the volume of pore water particles increases, reflecting the replenishment of water in simulating the freeze-thaw process.

Through the above analysis, it can be concluded that the fundamental reason for the deterioration during the freeze-thaw cycles is the volume expansion of internal pore water induced by the low-temperature. This expansion leads to the enlargement of the pore structure, requiring more water to replenish, ultimately resulting in the damage of the rock skeleton after repeated freeze-thaw actions. To quantify the frost heave degree of internal pore water particles during the freeze-thaw cycles, the frost heave evaluation index λ_v is defined as

$$\lambda_v = V_F^i / V_T^{i-1} \tag{10}$$

where V_F^i represents the volume after the freezing process of the i -th freeze-thaw cycle for pore water particles, and V_T^{i-1} denotes the volume after the thawing process of the $(i-1)$ -th freeze-thaw cycle for pore water particles.

The frost heave evaluation index (λ_v) of internal pore water particles is calculated with Eq. (10) every 5 freeze-thaw cycles, and the relationship between λ_v and the number of freeze-thaw cycles (N) can be described by an exponential function:

$$\lambda_v = -0.5979e^{-0.0611N} + 1.5615 \quad (R^2 = 0.9849) \tag{11}$$

As shown in Fig. 14, with the increase in the number of freeze-thaw cycles (N), the frost heave evaluation index (λ_v) exhibits an upward convex exponential change. Specifically, after 5, 10, 15, 20, 25, and 30 freeze-thaw cycles, λ_v increases by 14.12%, 22.50%, 35.29%, 41.25%, 44.29%, and 45.44%, respectively, compared to the condition without freeze-thaw treatment. Therefore, λ_v can serve as an evaluation index reflecting the frost heave degree of pore water particles during the freeze-thaw process.

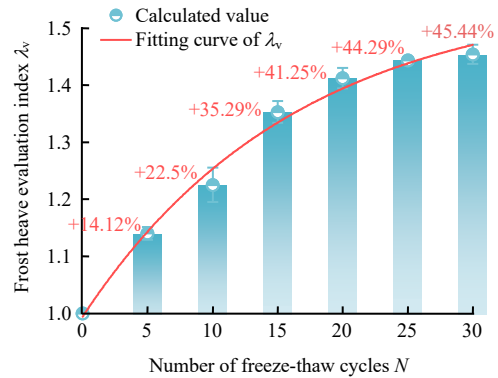


Fig. 14 Variation between frost heave index and number of freeze-thaw cycles

4.3 Loading-induced fracture evolution

The freeze-thaw process leads to interior deterioration of the rock, subsequently influencing the fracture characteristics under loading. Therefore, in this section, the relationship between the microcracks and the stress-strain curve in the simulation of freeze-thawed sandstone under uniaxial compression is analyzed. Meanwhile, the spatiotemporal fracture evolution of the sample is evaluated.

4.3.1 Stress-strain and microcrack evolution

The stress-strain curve is closely related to the microcrack evolution^[43]. Fig. 15 shows the curve of microcrack quantity varies with stress-strain. From Fig. 15(a), it can be seen that in the case without freeze-thaw treatment, the majority of microcracks are tensile cracks, with shear microcracks increasing in the later stages of loading but in a much smaller quantity. This indicates that tensile microcracks play a primary role in the failure of the sample with zero freeze-thaw cycles. According to Figs. 15(b) to 15(d), with an increase in the number of freeze-thaw cycles, the type of microcracks begins to transform under loading. After 10 and 20 freeze-thaw cycles, although the number of tensile microcracks is still higher than that of shear microcracks, a closer examination of the locally enlarged portion of the microcrack curve indicates that shear microcracks appear earlier and gradually increase compared to the condition with zero freeze-thaw cycles. After 30 freeze-thaw cycles, the number of shear microcracks

exceeds that of tensile microcracks, indicating that shear

microcracks dominate the failure of the sample.

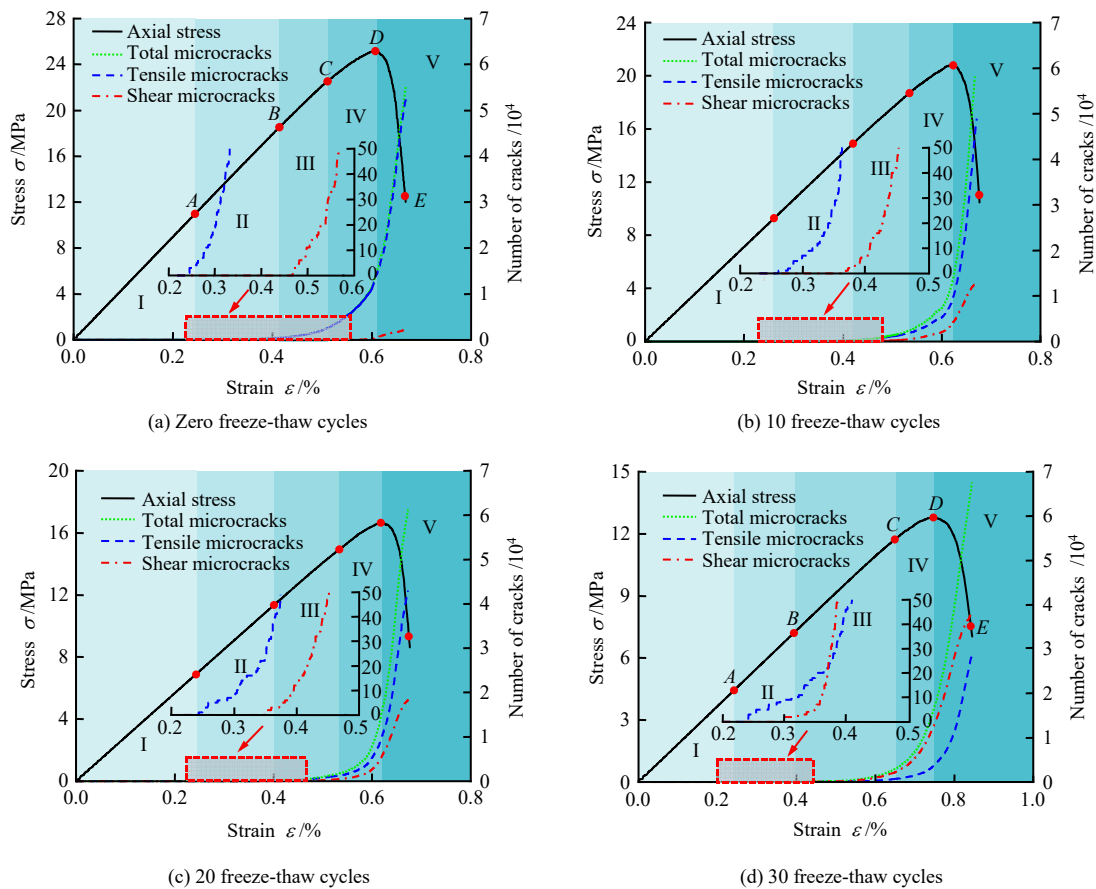


Fig. 15 Stress–strain curves and microcrack evolution of freeze-thawed sandstone

In summary, the overall evolution of microcracks follows a “slow–steady–rapid” development trend, and roughly can be categorized into five stages: no cracks (I), crack initiation(II), stable crack propagation (III), accelerated crack propagation (IV), and later-stage crack propagation (V).

Furthermore, the stress corresponding to the first appearance of microcracks is defined as the stress threshold of crack initiation^[44], and the tensile microcrack initiation stress σ_i^t , the shear microcrack initiation stress σ_i^s , and the peak stress σ_f are summarized in Table 3. From the table, it can be observed that as the number of freeze-thaw cycles increases from 0 to 10, 20, and 30, σ_i^t decreases by 15.57%, 37.25%, and 59.56%, respectively, while σ_i^s decreases by 41.74%, 56.17%, and 71.27%, respectively. This indicates that the cohesion of the rock skeleton is

Table 3 Microcrack initiation stress and peak stress of sample under uniaxial compression after freeze-thaw treatments

Number of freeze-thaw cycles N	Tensile microcrack initiation stress σ_i^t /MPa	Shear microcrack initiation stress σ_i^s /MPa	Peak stress σ_f /MPa
0	10.98	22.52	25.18
10	9.27	13.12	20.79
20	6.89	9.87	16.65
30	4.44	6.47	12.80

weakened by the repeated freeze-thaw treatments, allowing microcracks to initiate at lower stress and leading to a reduction in bearing capacity.

Additionally, Fig. 16 also shows the proportion of tensile and shear microcracks after loading. Specifically, as N increases to 10, 20, and 30 cycles, the proportion of tensile microcracks decreases by 17.4%, 25.6%, and 67.5%, respectively, compared to zero freeze-thaw cycles. Conversely,

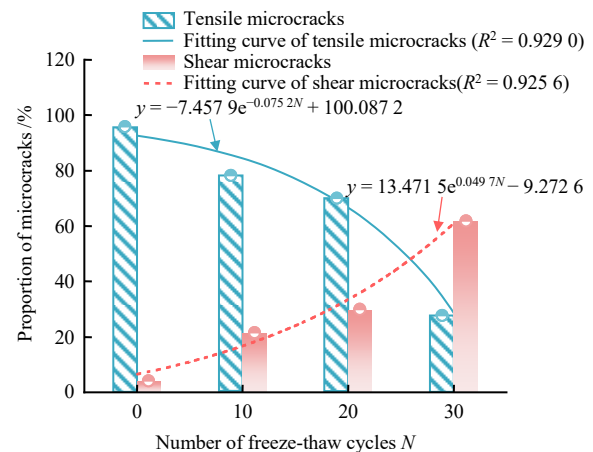


Fig. 16 Proportion of loading-induced tensile-shear microcrack quantity in samples under different numbers of freeze-thaw cycles

the proportion of shear microcracks increases by 17.4%, 25.6%, and 67.5%, respectively. Simultaneously, the ratio of tensile to shear microcracks after loading gradually decreases with increasing N , indicating that under the influence of freeze-thaw cycles, the dominant type of microcracks transforms after loading, thereby controlling the fracture mode.

To validate the reliability of the numerical results, the simulated results of freeze-thawed sandstone are compared with the laboratory test results (see Fig. 17). It is evident that the simulated peak strengths are relatively close to the experimental values, while there is some deviation in the peak strain. This is mainly attributed to the fact that laboratory samples are taken from natural rock masses and possess initial defects such as microcracks. Besides the influence of freeze-thaw cycles, the stress-strain curve of the sample has an inherent compaction stage under loading. Since the natural initial defects are difficult to be replicated by the numerical sample, there is some deviation in the simulated peak strains relative to the experimental results^[45]. Overall, the numerical results align well with the laboratory test results.

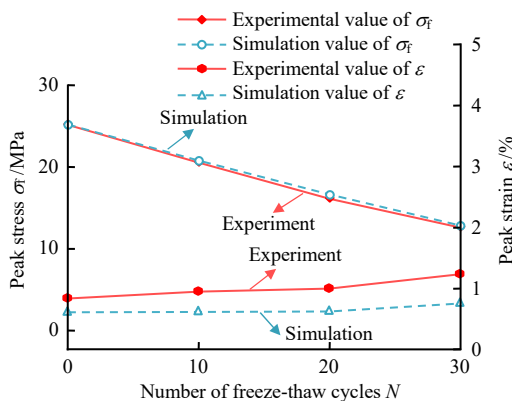


Fig. 17 Comparison between experimental and numerical results of freeze-thawed sandstone

4.3.2 Fracture evolution under loading

This section analyzes the asymptotic fracture process of freeze-thawed sandstone under loading using two samples subjected to 0 and 30 freeze-thaw treatments as examples. Figs. 18(a) and 18(b) illustrate the simulated fracture evolution for these samples, depicting the displacement field, force chain field, and microcrack distribution. The analysis of the fracture process is correlated with the loading stages marked as A , B , C , and D in Figs. 15(a) and 15(d).

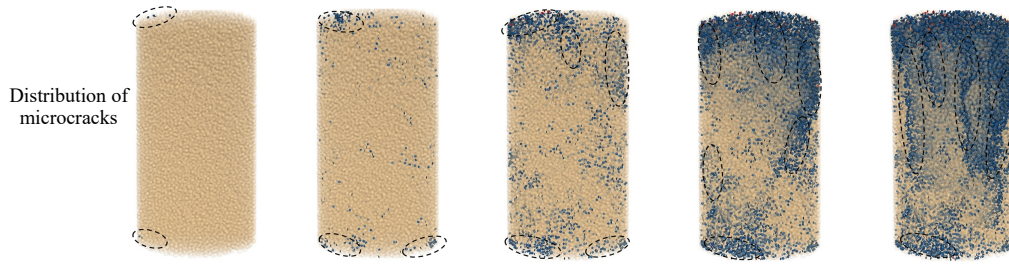
Stage before point A (I): There is no crack observed in both the samples under 0 and 30 freeze-thaw cycles before point A . The microcrack initiation stress (corresponding to point A) of the sample freeze-thawed 30 cycles is lower than that with 0 cycles, indicating that

the freeze-thaw cycles are prone to reduce the microcrack initiation stress, resulting in a reduced load-bearing capacity. From the displacement field, it is evident that both the samples freeze-thawed with 0 and 30 cycles are significantly compressed. From the force chain field, the direction of force transmission is predominantly vertical. (the force chains in the figure represent the transmission paths of external loads between particles, with thickness indicating force chain magnitude), is vertical.

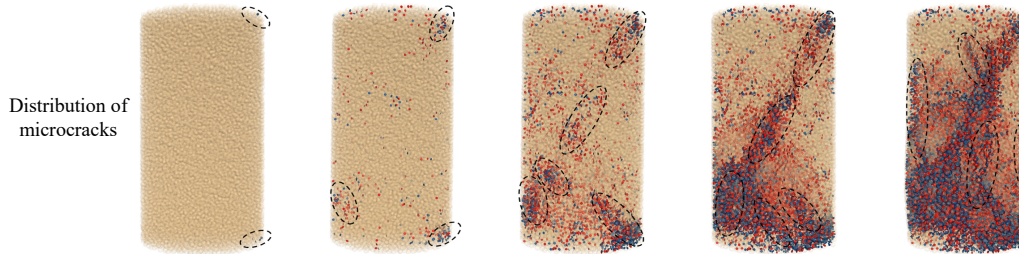
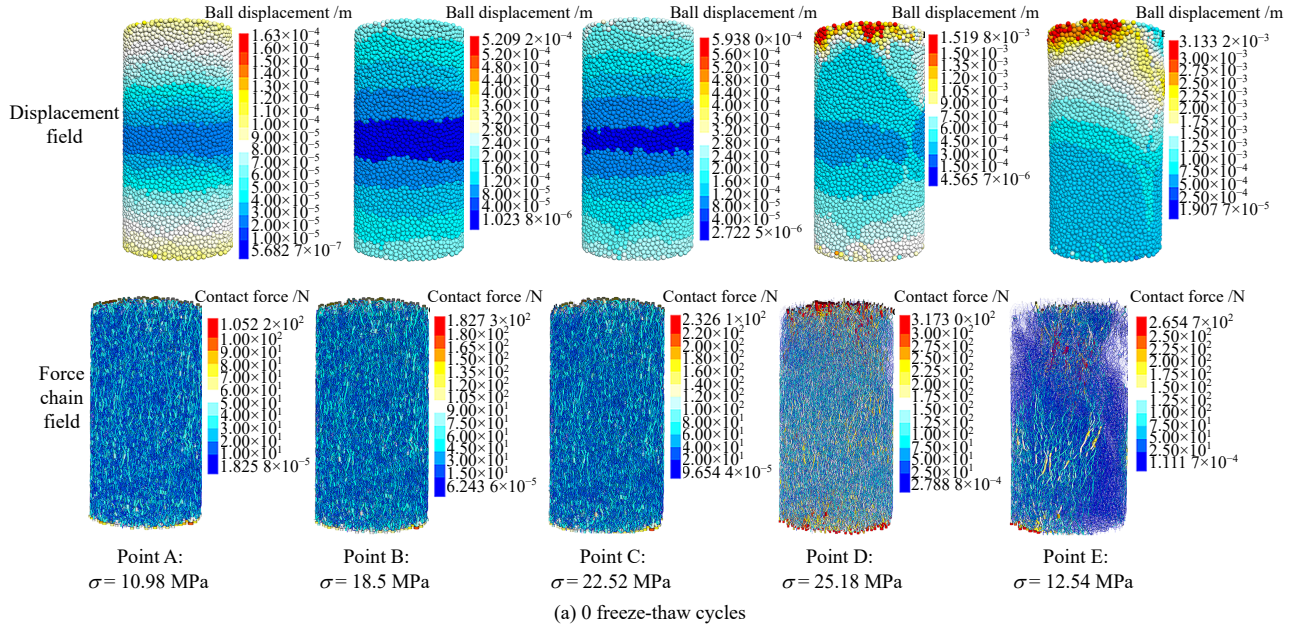
Stage A to B (II): Microcracks develop slowly during this stage. When loaded to point B , the microcrack patterns in the samples with 0 and 30 freeze-thaw cycles are completely different, and the locations of crack initiation also differ. Additionally, from the displacement and force chain fields of the sample with 0 cycles, it is observed that the maximum displacements of the upper and lower ends range from 1.6×10^{-4} to 2.4×10^{-4} m, with the maximum force chain value being 1.83×10^2 N. From the displacement and force chain fields of the sample with 30 cycles, the maximum displacements of the upper and lower ends range from 2.0×10^{-4} to 2.5×10^{-4} m, with a maximum force chain value of 81.8 N, indicating that the sample freeze-thawed 30 cycles is more prone to deforming under low loads.

Stage B to C (III): Microcracks develop steadily, and their growth rate is faster than that in the initiation stage (II). For the sample with 0 freeze-thaw cycles, when the axial stress reaches 22.52 MPa, clusters of tensile microcracks occur in the upper part of the sample. For the sample with 30 cycles, when loaded from point B to point C , shear microcracks grow significantly faster than tensile microcracks. When the stress reaches 11.74 MPa, shear microcracks mostly gather in the bottom and upper-right regions of the sample, serving as precursors to failure identification. Meanwhile, the force chain field indicates a significantly lower load-bearing capacity than that of the sample with 0 cycles.

Stage C to D (IV): Microcracks grow rapidly. For the sample with 0 freeze-thaw cycles, the tensile microcracks quickly develop and gather when approaching the peak stress. When reaching the peak stress of 25.18 MPa, significant microcrack clustering is observed at the top end, leading to fracture. The force chain field also indicates that the load-bearing capacity has reached its limit. For the sample with 30 cycles, there is a noticeable difference from the sample with 0 cycles. When loaded to the peak strength of 12.80 MPa, the microcracks at the upper-right and bottom parts of the sample undergo “clustering-propagation-coalescence”, forming an obvious fracture zone. In the fracture zone, tensile and shear microcracks



Note: the microcracks in blue represent tensile microcracks and the microcracks in red represent shear microcracks



Note: the microcracks in blue represent tensile microcracks and the microcracks in red represent shear microcracks

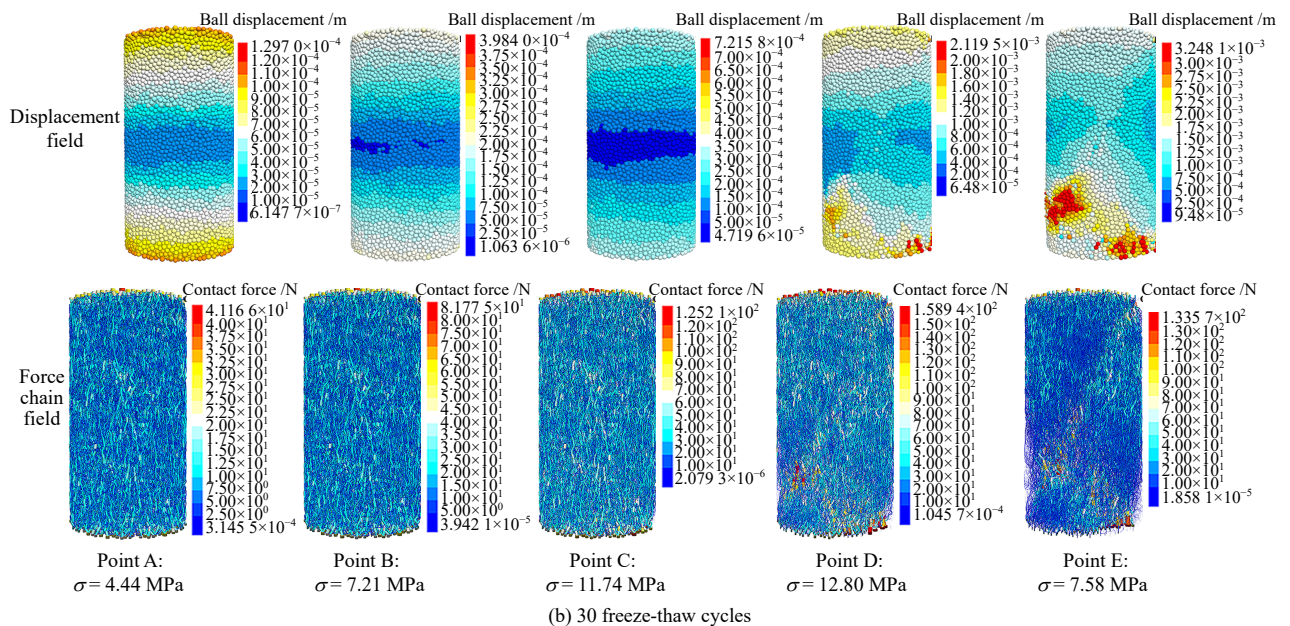


Fig. 18 Evolution of loading-induced fracture in samples

grow simultaneously and intersect each other. When approaching the peak stress (σ_f), both the samples with 0 and 30 cycles exhibit abnormal signals in internal microcrack distribution, displacement field, and force chain field, and the displacement and microcrack quantity are more than twice those of $0.9\sigma_f$, with a precursor of fracture occurring locally in the sample.

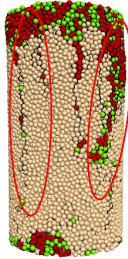
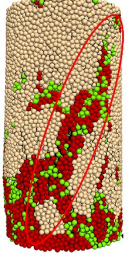
Stage *D* to *E* (*V*): At the post-peak stage, both the samples with 0 and 30 freeze-thaw cycles exhibit a sharp increase in microcracks. Specifically, when loaded to point *E*, there are multiple crack bands appearing along the axial direction of the sample with 0 cycles, with numerous microcracks gathering at the fracture location, forming a macroscopic fracture band. The displacement field shows a downward conical movement. From the force chain field, it is evident that the non-zero local force chains indicate a slight residual strength of the sample in the post-peak stage. For the sample with 30 cycles, when loaded to point *E*, macroscopic fracture features are more prominent, with secondary cracks propagating near the fracture band. The displacement field shifts upward and deviates toward the fracture location, and the post-peak force chain field is highlighted in the fracture region. These characteristics indicate that the sample has failed.

In summary, the loading-induced fracture processes of the samples significantly differ before and after cyclic freeze-thaw treatment. Comparing the results of 0 and 30 freeze-thaw cycles, it is apparent that the tensile fracture of the sample is primarily due to the extensive aggregation of tensile microcracks, and the shear fracture results from a fracture band composed of numerous shear and tensile microcracks. This suggests that under the influence of cyclic freeze-thaw treatment, the fracture mode transitions from being dominated by tensile microcracks to a mixed mode of tensile-shear microcracks, consistent with the results obtained by Zhang et al.^[46] using DIC technology. Additionally, when the sample fractures under loading after freeze-thawing, the spatial distribution of internal microcracks becomes more complex, and many secondary fractures are generated near the main fracture band. This observation highlights the significant impact of freeze-thaw cycles on the spatial distribution of microcracks, thereby exerting control over the macroscopic fracture pattern.

Table 4 presents the final failure modes of the samples with 0 and 30 freeze-thaw cycles. Through comparison, it can be found that the sample with 0 cycles mainly undergoes axial splitting failure, while the sample with 30 cycles exhibits an inclined (inclination angle is about 75°) shear fracture band extending across the entire sample from the top right end, with the bottom fractured severely. The numerical results align well with the fracture patterns

obtained by the laboratory tests, further validating the rationality of the loading-induced fracture process described above.

Table 4 Sample failure patterns without and with 30 freeze-thaw treatments

Number of freeze-thaw cycles N	Laboratory sample	Numerical sample
0		
30		

5 Conclusion

In this paper, combining the laboratory experiments, the mesoscopic damage and fracture process of freeze-thawed sandstone is investigated by the particle flow program. Based on the proposed method coupling water-ice particle phase transition and expansion, the cyclic freeze-thaw process of rocks is effectively simulated, the cumulative development of mesoscopic damage in rocks under freeze-thaw action is revealed, and the evolutionary behavior of loading-induced fracture in freeze-thawed rocks is analyzed thoroughly. The main conclusions are drawn as follows:

(1) During the freeze-thaw process, the microcracks in the sample are mainly dominated by tensile cracks, with higher crack density at the periphery than that in the interior. The number of microcracks shows an “initially slow, then fast” evolution trend, with more significant displacement of rock particles on the periphery than those in the interior. The volumetric expansion of pore water in the rock and continuous water replenishment are the essential causes of rock damage under freeze-thaw treatment. Additionally, with the increase in freeze-thaw cycles (N), λ_v exhibits a concave exponential variation and meets the relationship $\lambda_v = -0.5979e^{-0.0611N} + 1.5615$, which can serve as an evaluation index for frost heave degree.

(2) The evolution of microcracks during the loading process follows a “slow \rightarrow gradual \rightarrow rapid” growth trend. The number of freeze-thaw cycles (N) is positively correlated

with the number of loading-induced microcracks but negatively correlated with the tensile-shear microcrack initiation stress. As N increases, the ratio of tensile to shear microcracks after loading decreases.

(3) When the load approaches the peak stress (σ_f), abnormal signals are observed in the microcrack distribution, displacement field, and force chain field, and microcrack quantity are more than twice those of $0.9\sigma_f$. Moreover, the cyclic freeze-thaw process leads to a more complex spatial distribution of microcracks inside the sample, resulting in a transition from a fracture mode dominated by tensile microcracks to a mixed mode of tensile-shear microcracks.

(4) The sample with 0 cycles mainly undergoes axial fracture dominated by the tensile microcracks, while the sample with 30 cycles exhibits an inclined (inclination angle is about 75°) shear fracture band extending across the entire sample from the top right end. The shear fracture band is dominated by tensile and shear microcracks, with secondary fractures appearing near the main fracture band.

References

- [1] YANG C, ZHOU K, XIONG X, et al. Experimental investigation on rock mechanical properties and infrared radiation characteristics with freeze-thaw cycle treatment[J]. *Cold Regions Science and Technology*, 2021, 183: 103232.
- [2] WANG Z, WANG T, WU S, et al. Investigation of micro-cracking behaviors in brittle rock using polygonal grain-based distinct method[J]. *International Journal for Numerical and Analytical Methods in Geomechanics*, 2021, 45(13): 1871–1899.
- [3] QIAO Chen, LI Chang-hong, WANG Yu, et al. Experimental study on failure of central rock bridge under freeze-thaw cycle[J]. *Chinese Journal of Rock Mechanics and Engineering*, 2020, 39(6): 1094–1103.
- [4] DEPRez M, DE KOCK T, DE SCHUTTER G, et al. A review on freeze-thaw action and weathering of rocks[J]. *Earth-Science Reviews*, 2020, 203: 103143.
- [5] WANG P, XU J, FANG X, et al. Energy dissipation and damage evolution analyses for the dynamic compression failure process of red-sandstone after freeze-thaw cycles[J]. *Engineering Geology*, 2017, 221: 104–113.
- [6] TANG X, TAO S, LI P, et al. The propagation and interaction of cracks under freeze-thaw cycling in rock-like material[J]. *International Journal of Rock Mechanics and Mining Sciences*, 2022, 154: 105112.
- [7] LIU Jie, ZHANG Han, WANG Rui-hong, et al. Investigation of progressive damage and deterioration of sandstone under freezing-thawing cycle[J]. *Rock and Soil Mechanics*, 2021, 42(5): 1381–1394.
- [8] PENG Jian-bing, CUI Peng, ZHUANG Jian-qj, et al. Challenges to engineering geology of Sichuan-Tibet railway[J]. *Chinese Journal of Rock Mechanics and Engineering*, 2020, 39(12): 2377–2389.
- [9] ZHENG Guang-hui, XU Jin-yu, WANG Peng, et al. Physical characteristics and degradation model of stratified sandstone under freeze-thaw cycling[J]. *Rock and Soil Mechanics*, 2019, 40(2): 632–641.
- [10] LIU Bo, MA Yong-jun, SHENG Hai-long, et al. Experiments on mechanical properties of Cretaceous red sandstone after freeze-thaw process[J]. *Rock and Soil Mechanics*, 2019, 40(Suppl.1): 161–171.
- [11] TANG Ming-gao, XU Qiang, DENG Wen-feng, et al. Degradation law of mechanical properties of typical rock in Sichuan-Tibet Traffic Corridor under freeze-thaw and unloading conditions[J]. *Earth Science*, 2022, 47(6): 1917–1931.
- [12] LIU B, MA Y J, LIU N, et al. Investigation of pore structure changes in Mesozoic water-rich sandstone induced by freeze-thaw process under different confining pressures using digital rock technology[J]. *Cold Regions Science and Technology*, 2019, 161: 137–149.
- [13] MARTÍNEZ-MARTÍNEZ J, BENAVENTE D, GOMEZ-HERAS M, et al. Non-linear decay of building stones during freeze-thaw weathering processes[J]. *Construction and Building Materials*, 2013, 38: 443–454.
- [14] SONG Y, TAN H, YANG H, et al. Fracture evolution and failure characteristics of sandstone under freeze-thaw cycling by computed tomography[J]. *Engineering Geology*, 2021, 294: 106370.
- [15] JIANG De-yi, ZHANG Shui-lin, CHEN Jie, et al. Low field NMR and acoustic emission probability density study of freezing and thawing cycles damage for sandstone[J]. *Rock and Soil Mechanics*, 2019, 40(2): 436–444.
- [16] CHEN Yu-long, ZHANG Ke, SUN Huan. Meso-research on the development of rock surface crack under freeze-thaw cycles[J]. *China Civil Engineering Journal*, 2019, 52(Suppl.1): 1–7.
- [17] GU Xin-bao, ZHOU Xiao-ping. Numerical simulation of propagation and coalescence of cracks using peridynamic theory[J]. *Rock and Soil Mechanics*, 2017, 38(2): 610–616.
- [18] LIU Quan-sheng, WANG Zhong-wei. Review of numerical modeling based on digital image processing for rock mechanics applications[J]. *Chinese Journal of Rock Mechanics and Engineering*, 2020, 39(Suppl.2): 3286–3296.
- [19] JING L. A review of techniques, advances and outstanding issues in numerical modelling for rock mechanics and rock engineering[J]. *International Journal of Rock Mechanics and Mining Sciences*, 2003, 40(3): 283–353.
- [20] DING Z, FENG X, WANG E, et al. Acoustic emission response and evolution of precracked coal in the meta-instability stage under graded loading[J]. *Engineering Geology*,

- 2023, 312: 106930.
- [21] ZHOU Yang-shi-qi, ZHAO Lan-hao, SHAO Lin-yu, et al. A deformable spheropolygon-based discrete element method[J]. *Rock and Soil Mechanics*, 2022, 43(7): 1961–1968, 1977.
- [22] ZHOU Y, ZHAO D, LI B, et al. Fatigue damage mechanism and deformation behaviour of granite under ultrahigh-frequency cyclic loading conditions[J]. *Rock Mechanics and Rock Engineering*, 2021, 54(9): 4723–4739.
- [23] XIONG F, LIU X, ZHOU X, et al. Mechanical behaviours of sandstone containing intersecting fissures under uniaxial compression[J]. *Journal of Rock Mechanics and Geotechnical Engineering*, 2022, 14(2): 460–476.
- [24] BIAN Kang, CHEN Yan-an, LIU Jian, et al. The unloading failure characteristics of shale under different water absorption time using the PFC numerical method[J]. *Rock and Soil Mechanics*, 2020, 41(Suppl.1): 355–367.
- [25] WU Dong-yang, YU Li-yuan, SU Hai-jian, et al. Experimental study and PFC^{3D} simulation on crack propagation of fractured rock-like specimens with bolts under uniaxial compression[J]. *Rock and Soil Mechanics*, 2021, 42(6): 1681–1692.
- [26] ZHU T, CHEN J, HUANG D, et al. A DEM-based approach for modeling the damage of rock under freeze-thaw cycles[J]. *Rock Mechanics and Rock Engineering*, 2021, 54(6): 2843–2858.
- [27] China Electricity Council. GB/T 50266—2013 Standard for test methods of engineering rockmass[S]. Beijing: China Planning Press, 2013.
- [28] CHEN Ren-sheng, KANG Er-si, WU Li-zong, et al. Cold regions in China[J]. *Journal of Glaciology and Geocryology*, 2005(4): 469–475.
- [29] FAIRHURST C E, HUDSON J A. Draft of recommended method of ISRM for the determination of complete stress–strain curves of intact rock by uniaxial compression test[J]. *Chinese Journal of Rock Mechanics and Engineering*, 2000, 19(6): 802–808.
- [30] POTYONDY D O, CUNDALL P A. A bonded-particle model for rock[J]. *International Journal of Rock Mechanics and Mining Sciences*, 2004, 41(8): 1329–1364.
- [31] TOMAC I, GUTIERREZ M. Coupled hydro-thermo-mechanical modeling of hydraulic fracturing in quasi-brittle rocks using BPM-DEM[J]. *Journal of Rock Mechanics and Geotechnical Engineering*, 2017, 9(1): 92–104.
- [32] Itasca Consulting Group Inc. PFC 5.0 help manual[M]. Minneapolis: Itasca Consulting Group Inc, 2014.
- [33] LIU C, DENG H, CHEN X, et al. Impact of rock samples size on the microstructural changes induced by freeze-thaw cycles[J]. *Rock Mechanics and Rock Engineering*, 2020, 53(11): 5293–5300.
- [34] LIU Quan-sheng, HUANG Shi-bing, KANG Yong-shui, et al. Study of unfrozen water content and frost heave model for saturated rock under low temperature[J]. *Chinese Journal of Rock Mechanics and Engineering*, 2016, 35(10): 2000–2012.
- [35] YAN Jian, HE Chuan, ZENG Yan-hua, et al. Strong cold wind environment outside extra-long tunnel in high-altitude region and its influence on temperature field of surrounding rock structure[J]. *China Journal of Highway and Transport*, 2019, 32(11): 192–201.
- [36] DENG Shu-xin, ZHENG Yong-lai, FENG Li-po, et al. Application of design of experiments in microscopic parameter calibration for hard rocks of PFC^{3D} model[J]. *Chinese Journal of Geotechnical Engineering*, 2019, 41(4): 655–664.
- [37] SHI Z, LI J, WANG J, et al. Experimental and numerical study on fracture characteristics and constitutive model of sandstone under freeze-thaw-fatigue[J]. *International Journal of Fatigue*, 2023, 166: 107236.
- [38] LIN H, LEI D, ZHANG C, et al. Deterioration of non-persistent rock joints: a focus on impact of freeze-thaw cycles[J]. *International Journal of Rock Mechanics and Mining Sciences*, 2020, 135: 104515.
- [39] TAN Hao, SONG Yong-jun, GUO Xi-xi, et al. Research on meso-damage and strain localization of fractured sandstone after freeze-thaw cycles[J]. *Chinese Journal of Rock Mechanics and Engineering*, 2022, 41(12): 2485–2496.
- [40] WINKLER E M. Frost damage to stone and concrete: geological considerations[J]. *Engineering Geology*, 1968, 2(5): 315–323.
- [41] HUANG C, ZHU C, MA Y, et al. Investigating mechanical behaviors of rocks under freeze-thaw cycles using discrete element method[J]. *Rock Mechanics and Rock Engineering*, 2022, 55(12): 7517–7534.
- [42] SUN Y, ZHAI C, XU J, et al. Characterisation and evolution of the full size range of pores and fractures in rocks under freeze-thaw conditions using nuclear magnetic resonance and three-dimensional X-ray microscopy[J]. *Engineering Geology*, 2020, 271: 105616.
- [43] SONG Yong-jun, CHENG Ke-yan, MENG Fan-dong. Research on acoustic emission characteristics of fractured rock damage under freeze-thaw action[J]. *Chinese Journal of Mining and Safety Engineering*, 2023, 40(2): 408–419.
- [44] ZHANG L, REN T, LI X, et al. Acoustic emission, damage and cracking evolution of intact coal under compressive loads: experimental and discrete element modelling[J]. *Engineering Fracture Mechanics*, 2021, 252: 107690.
- [45] ZHAO H, ZHANG L, WU Z, et al. Fracture mechanisms of intact rock-like materials under compression[J]. *Computers and Geotechnics*, 2022, 148: 104845.
- [46] ZHANG Q, LIU Y, DAI F, et al. Experimental assessment on the fatigue mechanical properties and fracturing mechanism of sandstone exposed to freeze-thaw treatment and cyclic uniaxial compression[J]. *Engineering Geology*, 2022, 306: 106724.